SIMULATION OF GUIDED WAVE PROPAGATING IN COMPOSITE LAMINATES WITH A FAST FINITE ELEMENT-BASED METHOD

Xing Kou[1, 2], Emanuele Casciaro[2], Cheng Qian[1], Cuixiang Pei[1], Paolo Bettini[2] and Zhenmao Chen[1]

[1] State Key Lab. for Strength and Vibration of Mechanical Structures, Shaanxi Engineering Research Center for NDT and Structural Integrity Evaluation, Xi'an Jiaotong University, Xi'an, China
[2] dept. of Aerospace Science and Technology, Politecnico di Milano, Milano, Italy
Email: xing.kou@polimi.it, emanuele.casciaro@polimi.it, qiancheng1999@stu.xjtu.edu.cn, pei.cx@mail.xjtu.edu.cn, paolo.bettini@polimi.it, chen.zm@mail.xjtu.edu.cn

Keywords: Guided wave, Composite plates, Simulation, Finite element method

ABSTRACT

Guided wave propagation constitutes a promising physical approach for the structural health monitoring of composites in aerospace applications. An efficient and reliable numerical simulation on guided wave propagating in composites is highly valuable as it offers both theoretical reference and technological support. As a commonly used approach, the time-explicit algorithm with the Finite element method (FEM) could be coded to implement simple algebraic equations instead of solving the inversion of large matrices. However, due to the restriction of spatial and temporal discretization, it is memory and computation expensive for 3D composite laminate problems. In this paper, a fast dynamic explicit FEM-based simulation method is developed using a one-dimensional compressing data storage technique to reduce memory and computational cost. The method is applied to simulate guided waves in a glass fiber-reinforced polymer cross-ply laminate. Firstly, the analytical disperse solution in multi-layers plates is obtained based on the stiffness matrix method (SMM) with the assumption of transversely isotropic in each ply. Then, the COMSOL/Explicit package is used to simulate the same model as the fast FEM-based simulation. The results show that the proposed method offers a significant reduction in computation time and storage capacity, making it an efficient and reliable tool for simulating guided waves in composites. Afterward, the accuracy of the fast FEM-based method for each propagation direction is verified with the comparison to analytical disperse solutions by wavenumber analysis. Finally, the predicted signal from the proposed method is validated by experiments.

1 INTRODUCTION

Elastic guided wave (GW), which is widely used in structural health monitoring of composite material [1-5], is susceptible to material degradation with long distance and low attenuation detection capability. In flat plates, GWs travel as Lamb waves, which are vertically polarized, and shear horizontal (SH) waves, which are horizontally polarized. Lamb waves are classified as symmetric (S) and anti-symmetric (A) waves based on the symmetric and anti-symmetric behaviour of the mode shape to the mid-plane. With multi-mode characteristics, the guided waves are denoted as Sn, An, and SHn with the subscript n=0,1,2,…. For the SH waves, even and odd subscripts represent the symmetric and anti-symmetric SH modes [6]. Below the cut-off frequency value (depending on the frequency-thickness product, and generally lies in the 0.5 and 1 MHz·mm range for composite), only two basic Lamb wave modes exist: S0, which is a symmetrical Lamb wave at low frequencies, similar to a longitudinal wave; and A0, which is an anti-symmetrical flexural wave at low frequencies. Due to the typically high damping values in such material [7], the majority of reported studies on GW detection in composites have been carried out under cut-off frequencies, focusing on the A0, S0, and SH0 modes.

Effective numerical simulation is needed to analyse the GW propagation in the given composite, as well as the interaction with imperfect boundaries or defects caused by material degradation. For the three-dimensional (3D) simulation of GWs in composite, many numerical methods have been investigated and most of them are based on the finite element method (FEM) [8-11], finite difference method (FDM) [12], spectral element method (SEM) [13], and finite integration technique (FIT) [14]. Among these methods, FEM is the most popular numerical approach for solving differential equations

by utilization of subdomains and has become an industry standard to solve practical complicated engineering problems. Nowadays, FEM is the most used numerical approach to investigate GWs in composite plates.

For finite element (FE) simulation of multi-layer material, the continuum-based three-dimensional (3D) elasticity method can capture the entire wave motion types accurately and efficiently, compared to other approaches such as equivalent single layer and layer-wise methods. For FE analysis of GW propagation, there are two main approaches: the explicit and the implicit schemes. The 3D problem introduces a large number of DOFs that depends on the number of layers constituting the laminate and results in low calculation efficiency in large implicit FE simulations, which can be extremely computationally expensive due to the required inversion of the mass matrix. Explicit FE schemes do not suffer this inversion drawback and can be coded to implement simple algebraic equations. To avoid numerical instability, the element dimension should be smaller than the minimum wavelength, and the time step must be less than the wave propagation time across a single element [7]. Both explicit and implicit schemes are used by most commercial software and have been adopted in many studies. Reference [10] presented 3D modelling of GWs in carbon fiber reinforced polymer (CFRP) laminates with four commercial FE tools: Ansys/Implicit, COMSOL/Implicit, Abaqus/Implicit, and Abaqus/Explicit. Benchmark comparisons are made between the simulation tools, as well as experimental data and theoretical dispersion curves, to evaluate their computational performance. Reference [11] used Abaqus/Implicit and Abaqus/Explicit software packages to simulate GW propagation in composite panels. In comparison to the experimental dataset, the results proved that both implicit and explicit schemes can provide accurate results. The explicit method is preferable, due to the considerably reduced computational costs. However, with the restriction of spatial and temporal discretization, the challenge for time-explicit FEM analysis is the memory and computation costs, especially for the 3D composite laminate problem.

Hence, to reduce memory and computational costs, a fast dynamic explicit FEM-based simulation method, faster than the commercial ones, is developed for the GW propagation in composite plates. The one-dimensional compressing data storage technique is used to reduce the required memory capacity, which only stores the nonzero elements in the coefficient matrixes. Firstly, the disperse characteristics in multi-layers plates are obtained based on the stiffness matrix method (SMM) with the assumption of transversely isotropic in each ply. Then, the COMSOL/Explicit package is used to simulate the same model as the fast FEM-based simulation. The results show that the proposed method offers a significant reduction in computation time and in the required storage capacity. Afterward, by 3D fast Fourier Transformation, the accuracy of the fast FEM-based method for each propagation direction is verified with the comparison to analytical disperse solutions, in the wavenumber domain. Finally, the signal predicted by the proposed method is compared with the experiment result, to validate the efficiency and reliability of the method.

2 THEORY AND NUMERICAL METHOD

2.1 Elastic guided wave in multi-layer composite

In the multi-layer model, the composite laminate is composed of N transversely isotropic plies, as shown in Fig. 1. The propagation direction of the GW is set as x axis, while the thickness direction is z. The density, thickness, and elastic constants of the n-th layer are $\rho^{(n)}$, $d^{(n)}$, and $\mathbf{D}^{(n)}$. The wave equation of the plate is given by:

$$D_{ijkl}\frac{\partial^2 u_k}{\partial x_j \partial x_l} = \rho \frac{\partial^2 u_i}{\partial t^2} \tag{1}$$

where u_i is the components of displacement. The motion can generally have three nonzero spatial components u_x, u_y and u_z, where u_y corresponds to SH wave, while u_x and u_z corresponds to lamb waves. The particle motions for Lamb and SH modes are uncoupled if propagation occurs along an in-plane axis of symmetry [15].

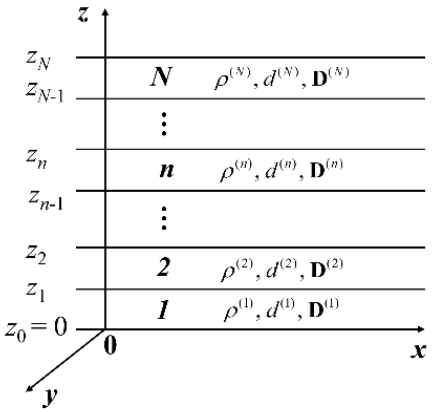

Figure 1: The multi-layer model.

Given that the axial direction of fiber is along *x* direction, each ply in the model in *y*-*z* plane can be considered transversely isotropic. The single-layer is rotated of an angle θ counterclockwise along the axis *z*, then the stiffness matrix of *n*-th layer with different arrangement angle is:

$$\mathbf{D}^{(n)} = \mathbf{M}\mathbf{D}^{\mathbf{0}}\mathbf{M}^{T} \tag{2}$$

The specific expression of the stiffness matrix, before rotated $\mathbf{D}^{\mathbf{0}}$, and the transformation matrix $\mathbf{M}$ are reported in [16].

In the *n*-th layer, the displacement of wave $(u_x^{(n)}, u_y^{(n)}, u_z^{(n)})$ can be expressed as follows:

$$(u_x^{(n)}, u_y^{(n)}, u_z^{(n)}) = (U_x^{(n)}, U_y^{(n)}, U_z^{(n)}) \exp(ik(x + \alpha^{(n)} z - c_p t)) \tag{3}$$

where *k* is the *x*-component of the wave number, *i* is the imaginary units, α denotes the ratio of wave number along axis *z* and *x*, $(U_x^{(n)}, U_y^{(n)}, U_z^{(n)})$ are constants, c_p is the phase velocity along axis *x* which is given by $c_p = \omega / k$, and ω is the angular frequency.

GWs have distinct disperse characteristics, which means the propagation velocities and mode shapes are frequency dependent. There are serval methods to calculate the dispersion curves in multi-layer composites. Considering the numerical stability and calculation efficiency [6], the SMM is used to obtain the disperse curves in this paper. In the SMM method, the relationship in the *n*-th layer can be written as [17]:

$$\begin{Bmatrix} \boldsymbol{\sigma}_-^{(n)} \\ \boldsymbol{\sigma}_+^{(n)} \end{Bmatrix} = \begin{bmatrix} K_{11}^{(n)} & K_{12}^{(n)} \\ K_{21}^{(n)} & K_{22}^{(n)} \end{bmatrix} \begin{Bmatrix} \mathbf{u}_-^{(n)} \\ \mathbf{u}_+^{(n)} \end{Bmatrix} \tag{4}$$

Matrix $\mathbf{K}^{(n)}$ contains the coefficients associated with stresses, displacements, and the thickness of *n*-layer.

Considering the continuity of the displacements and stress components at the interface of the layers, the global stiffness matrix can be obtained recursively. This matrix relates the stresses to the displacement from the top and bottom surface of the whole composite laminate:

$$\begin{bmatrix} \mathbf{K}_{11}^{(n)} + \mathbf{K}_{12}^{(n)} \left(\mathbf{K}_{11}^{(n+1)} - \mathbf{K}_{22}^{(n)} \right)^{(-1)} \mathbf{K}_{21}^{(n)} & -\mathbf{K}_{12}^{(n)} \left(\mathbf{K}_{11}^{(n+1)} - \mathbf{K}_{22}^{(n)} \right)^{(-1)} \mathbf{K}_{12}^{(n+1)} \\ \mathbf{K}_{21}^{(n+1)} \left(\mathbf{K}_{11}^{(n+1)} - \mathbf{K}_{22}^{(n)} \right)^{(-1)} \mathbf{K}_{21}^{(n)} & \mathbf{K}_{22}^{(n+1)} - \mathbf{K}_{21}^{(n+1)} \left(\mathbf{K}_{11}^{(n+1)} - \mathbf{K}_{22}^{(n)'} \right)^{(-1)} \mathbf{K}_{12}^{(n+1)} \end{bmatrix} \tag{5}$$

Assuming that the stress components are free on the uppermost and lowermost surfaces of the plate, the guided wave dispersion equation is:

$$\det(\mathbf{K}) = 0 \tag{6}$$

2.2 Finite element method with explicit integration

In the absence of an external force, the governing equation can be expressed in matrix form as:

$$[\nabla]^T [D][\nabla]\{u\} + \{f\} = \rho\{\ddot{u}\} + \gamma\{\dot{u}\} \tag{7}$$

where $[D]$ is the stiffness matrix which can be obtained from Equation (2), $\{u\}$ is the displacement vector, $\{f\}$ is the external force vector, $[\nabla]$is the gradient matrix function, γ is the acoustic damping coefficient.

The boundary conditions on the solid surfaces are:

$$[n]^T \{\sigma\} = \{\hat{t}\} \ \ (On\ surface) \tag{8}$$

where, $\{\hat{t}\} = \{\hat{t}_x, \hat{t}_y, \hat{t}_z\}^T$ is the external force tensor loading on the solid surface.

In addition to boundary conditions, the initial condition for the elastic wave field is:

$$\{u\}\big|_{t=0} = \{\dot{u}\}\big|_{t=0} = 0 \tag{9}$$

For the 3D simulation, the eight-node hexahedral isoperimetric elements can be used in a discrete model. Based on the weighted residual method, the differential governing equation of the elastic wave field can be transformed into an integration form. According to the principle of the partial integration method, and considering the boundary condition, the element governing equation can be given as:

$$\left[M^e\right]_{24\times24}\left\{\ddot{U}\right\}_{24\times1} + \left[D^e\right]_{24\times24}\left\{\dot{U}\right\}_{24\times1} + \left[G^e\right]_{24\times24}\left\{U\right\}_{24\times1} = \left\{F^e\right\}_{24\times1} \tag{10}$$

The element mass matrix, damping matrix, stiffness matrix, and force vector are expressed as:

$$\left[M^e\right]_{24\times24} = \rho\int_{-1}^{1}\int_{-1}^{1}\int_{-1}^{1}[N]_{24\times3}^T[N]_{3\times24}|J|d\xi d\eta d\zeta \tag{11}$$

$$\left[D^e\right]_{24\times24} = \gamma\int_{-1}^{1}\int_{-1}^{1}\int_{-1}^{1}[N]_{24\times3}^T[N]_{3\times24}|J|d\xi d\eta d\zeta \tag{12}$$

$$\left[G^e\right]_{24\times24} = \int_{-1}^{1}\int_{-1}^{1}\int_{-1}^{1}[B]_{24\times6}^T[D]_{6\times6}[B]_{6\times24}|J|d\xi d\eta d\zeta \tag{13}$$

$$\left[F^e\right]_{24\times1} = \int_{-1}^{1}\int_{-1}^{1}\int_{-1}^{1}[N]_{24\times3}^T\{F\}_{3\times1}|J|d\xi d\eta d\zeta \tag{14}$$

where ξ, η, ζ are the natural coordinates in the master element, N_i is the shape function, [J] is the Jacobi matrix, $[B]_{6\times24} = [\partial]_{6\times3}[N]_{3\times24}$.

Gauss quadrature is applied in generating element matrices. This method locates sampling points and assigns weights to minimize integration error when the integrand is a general polynomial. Based on the concept of FEM, after assembling the element governing equation, the global governing equation of the 3D elastic wave field can be described as:

$$[M]\left\{\ddot{U}\right\} + [D]\left\{\dot{U}\right\} + [G]\{U\} = \{F\} \tag{15}$$

Where, [M], [D], and [G] are the global mass matrix, damping matrix, and stiffness matrix; {F}is the external force vector applied on the discrete model. The mass of the element is assumed to be distributed to each node of the element, which means the element mass matrix is transformed into a diagonal matrix. [18].

The FEM-formed global governing equation is established at a particular time t. To obtain the entire time history of the generalized ultrasonic field, time-domain integration over the whole time is needed. The existing integration algorithms can be divided into implicit and explicit methods. With the time-implicit algorithm, it will take very huge memory and computation costs to solve the linear equation,

even in a small model, as the dimension of the sparse coefficient matrixes for the elastic wave field is very huge. The explicit algorithm does not suffer this drawback and can be coded to calculate algebraic equations. In our simulation, the time-explicit integration algorithm based on the central difference method and Newmark average velocity method is used, which has more than second-order accuracy to meet the needs of practical engineering applications [19].

$$\begin{cases} \{\dot{U}\}_{t+\Delta t} = \{\dot{U}\}_{t-\Delta t} - 2\Delta t[M]^{-1}\left[[D]\{\dot{U}\}_t + [G]\{U\}_t - \{F\}_t\right] \\ \{U\}_{t+\Delta t} = \{U\}_t + \left[\{\dot{U}\}_{t+\Delta t} + \{\dot{U}\}_t\right]\Delta t / 2 \end{cases} \tag{16}$$

Therefore, the displacement field can be directly calculated with less consumed time and storage. For the convergence of the explicit integration algorithm, the element size should be smaller than $\lambda_{min}/10$, where λ_{min} is the shortest wavelength of interest. Meanwhile, the time step should be smaller than l_{min}/C_l, where l_{min} *is* the fastest wave in the material.

To further reduce the amount of storage capacity and calculation cost, the explicit integration algorithm is combined with the non-zero element one-dimensional compressed storage method , as the damping and stiffness matrices are sparse. Only the non-zero elements in the matrices and their corresponding locations are stored, to calculate the required displacement field. The storage capacity is highly reduced compared with the traditional half-bandwidth storage method. This provides an improvement in calculation efficiency.

3 NUMERICAL MODEL AND EXPERIMENT SETUP

3.1 Numerical model

The combination of the time-explicit integration algorithm and the one-dimensional compressed storage method enables the development of a memory-efficient code, which could perform a larger three-dimensional (3D) model than current commercial tools. With the feature of high-performance computing, the FORTRAN language is used to implement the numerical program. The custom fast FEM-based program and COMSOL/Explicit commercial package are used to simulate the interested guided wave in a glass fiber reinforced polymer (GFRP) cross-ply laminate. The attenuation caused by material damping is not considered in the models. The comparison of the two models is used to verify the efficiency and accuracy of the fast FEM-based method.

Table 1 lists the material properties of the GFRP composite (3M's unidirectional SP250 S29A) used in the models, with the assumption of transversely isotropic in each ply. The layout of the composite material is $[0/90]_s$ with a total thickness of 1.6 mm, which matches the measured value of the experimental specimens.

Property	Symbol	Value
Density (kg·m^{-3})	ρ	1.88×10^3
Young's moduli (GPa)	E_1	45.7
	E_2 (=E_3)	13.5
Shear moduli (GPa)	G_{12} (=G_{13})	5.41
	G_{23}	5.19
Poisson's ratios	v_{12} (=v_{13})	0.27
	v_{23}	0.42

Table 1: Mechanical properties.

The disperse curves of the group velocity are obtained based on SMM. Fig. 2 shows both symmetric and anti-symmetric modes of propagating Lamb wave in the GFRP cross-ply. Only basic (in solid line) and first-order (in dotted line) modes are plotted, as the basic modes generated under a low frequency-thickness product are used in this paper.

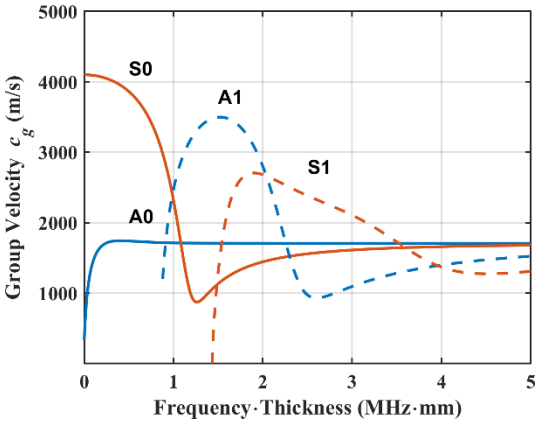

Figure 2: Dispersion curves of group velocity.

The excitation frequency f_0 is set as below 300 kHz in this paper, at which only the symmetric S0 mode and anti-symmetric A0 mode are generated. The proposed fast FEM-based simulation is performed to simulate an area of 100 mm × 100 mm as Fig. 3 (a) shows. All edges are set as stress-free boundaries. The probe points are set as a 41×41 array with a spacing of 2×2 mm for two-dimensional wavenumber analysis. For the commercial package, to reduce memory cost, a simplified model (45 mm × 10 mm area) in Fig. 3 (b) is established by the Elastic Waves- Time Explicit Interface in COMSOL, with the setting of the absorbing layers and symmetric boundaries. A single probe point is set in the COMSOL model, to collect displacement signals and compare them with that obtained by the probe point which has the same propagation distance (40 mm) in the fast-FEM model.

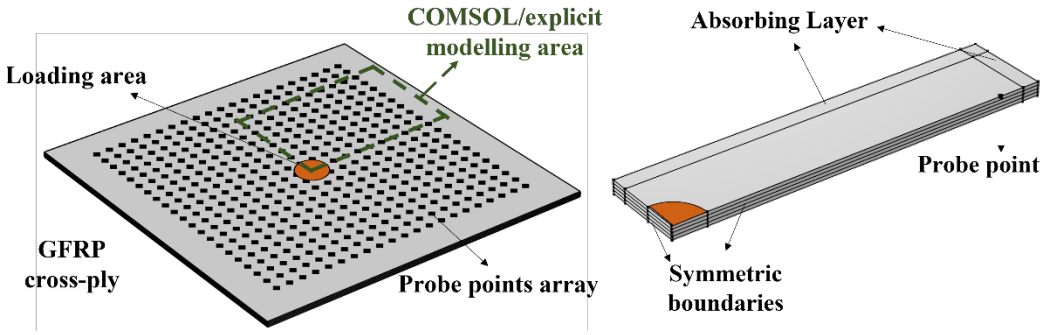

(a) (b)

Figure 3: Established numerical model of (a) fast FEM-based program and (b) COMSOL/Explicit.

The 3-cycle sinusoidal tone-burst signal with Hanning-window is incident normally over a 4-mm diameter circular on the surface. The expression of the loading $P(t)$ can be written as:

$$P(t)=\begin{cases} q\cdot\sin\left(2\pi f_0 t\right)\cdot\left(0.54-0.46*\cos\left(2\pi f_0 t/3\right)\right), & 0\le t\le 3/f_0 \\ 0, & t>3/f_0 \end{cases} \tag{17}$$

where q is the amplitude of the excitation signal, and f_0 is the excitation frequency.

Considering the convergence condition, as well as the element distortion due to high aspect ratios in the 3D FEM model, the maximum in-plane element dimension is set as 0.4 mm × 0.4 mm for the fast FEM-based model and 0.8 mm × 0.8 mm for the COMSOL model. In the thickness direction, two elements are set in each plyfor all the models. For the simplified model in COMSOL, the quartic shape functions are used, and the physical thickness of the absorbing layer contains 3 mesh elements. The fixed time step size is set as Δt = 0.03 μs.

3.2 Experiment setup

A GFRP panel (3M's unidirectional SP250 S29A) with the same layout and overall thickness as the simulation is fabricated, with the size of 434 mm × 60 mm. To excite and receive guided waves in the panel, two Ferroperm Pz27 piezoceramic plates are bonded by a two-component epoxy on the central line of the surface symmetrically as both actuator and sensor. The dimension of the Pz27 plate is 30 mm × 30 mm × 0.5 mm. The distance between the two Pz27 plates is 114 mm. To drive the actuator, a signal generator (LeCroy Wave Station 2052) is used and generates a tone-burst signal with a central frequency of 100 kHz and peak-to-peak voltage of 4 V. The signal type is the same as in the simulation. The signal received by the sensor is amplified by a high-voltage amplifier (Elba Tech T-506) and then recorded by an oscilloscope (Agilent Technologies DSO-X 2024A). The experiment setup is shown in Fig. 4.

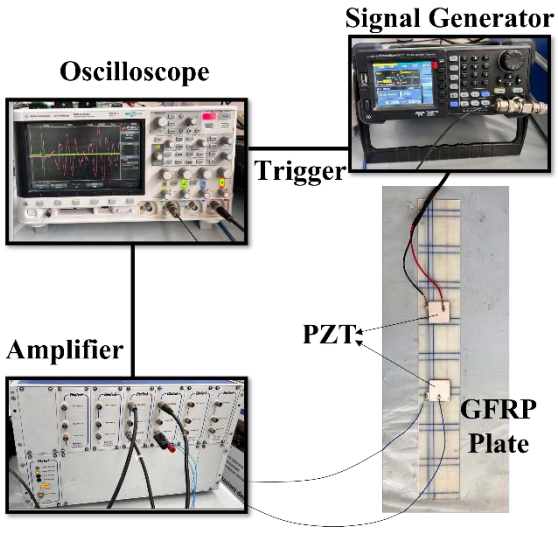

Figure 4: Experiment setup.

4 RESULTS AND DISCUSSION

4.1 Comparison with COMSOL/Explicit results

The excitation frequency is set at 300 kHz to investigate the performance of the two numerical approaches. The calculation total time is T_{sim} = 36 μs. Figure 5 shows the simulated wave field at a time of 18 μs in a grayscale map. The amplitude of the particle oscillation velocity is denoted in the color bar. Both A0 mode and S0 mode can be distinguished in Fig. 5 (a). Under low frequency-thickness product excitation, the motion of particles at S0 mode is mainly in-plane, while that at A0 mode is mainly out-plane. As the displacement generated by a normal incident force is mainly out-of-plane, the amplitude

of the obtained A0 mode is much bigger than the S0 mode. In the wave field resulting from the simplified COMSOL model, the A0 mode also can be identified, as shown in Fig. 5 (b).

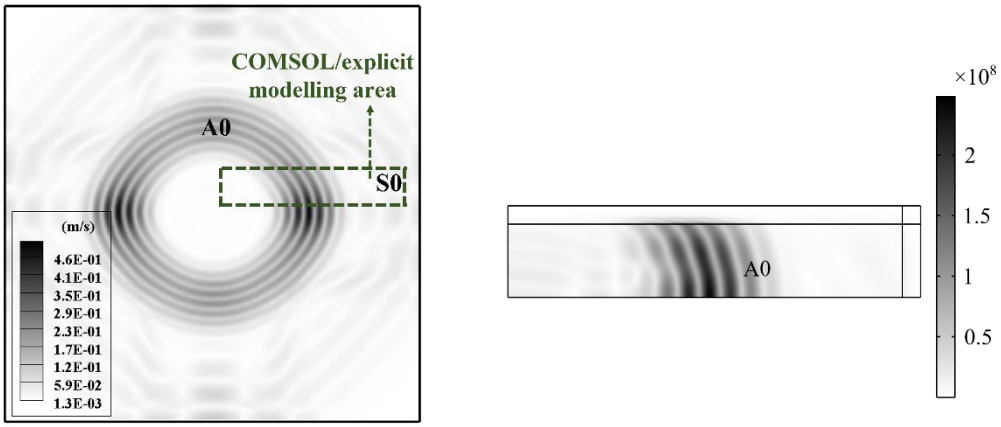

(a) (b)

Figure 5: The simulated wave field from (a) fast FEM-based program and (b) COMSOL/Explicit.

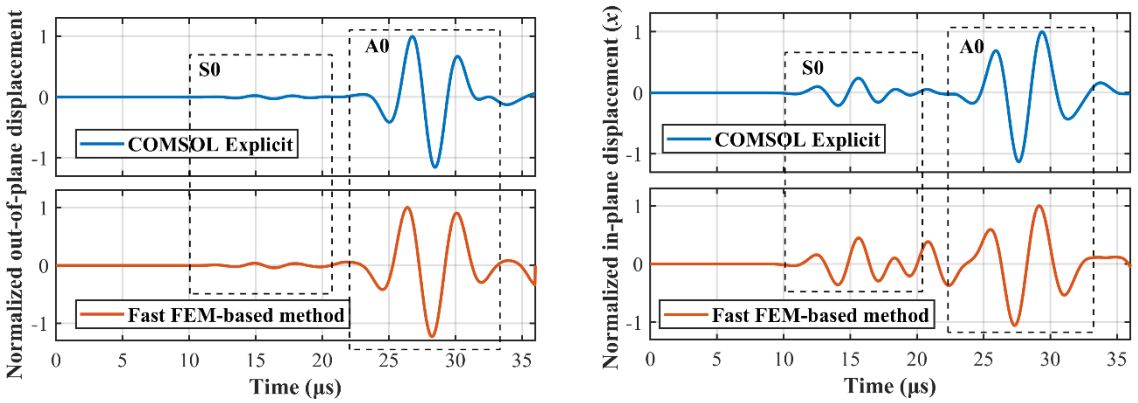

(a) (b)

Figure 6: The comparison of the (a) in-plane and (b) out-of-plane displacement signals

The comparison of the in-plane displacement (along the *x*-axis) and out-of-plane displacement is shown in Fig. 6. All the curves are normalized by the maximum value. The arriving time and waveforms of both S0 and A0 modes are nearly consistent with each other. The main reason for the existence of the small difference is that the absorbing layer is set in the simplified COMSOL model, which means there is almost no reflection wave by the boundaries.

The cross-correlation method is applied to the signals in Fig. 6 (b) to determine the arriving times of S0 and A0 mode, which means the value of the time instant for which the cross-correlation integral of the received signals and excitation signals reaches a maximum. The relative errors δ are obtained with the calculated velocities from models and reference velocities from the disperse curve, in which the theoretical S0 and A0 velocities are around 3883 m/s and 1740 m/s. The results are in Tab. 2. The calculated wave velocities from both the fast FEM-based code and commercial package are in good agreement with the theoretical values.

Table 2 also shows the performance of the two approaches. The number of Degrees of Freedom (DoF) is estimated with the product of nodes number and the number of displacement variables. Even calculating a model with 7 times DoF more than commercial software, the proposed fast-FEM program is much more efficient. The calculation running time (T_{run}) of the proposed method is only several minutes, while requires many hours in the commercial software. And the storage capacity (Mem) is 10 times less than it.

	Metric	Approach	
		Fast FEM-based method	COMSOL/ Explicit
Velocity	v_{S0} (m/s)	3745.3	3777.1
	δ_{S0} (%)	-3.5	-2.7
	v_{A0} (m/s)	1784.9	1768.3
	δ_{A0} (%)	+2.6	+1.6
Performance	Δt (μs)	0.03	0.03
	T_{sim} (μs)	36	36
	DoF (10^2)	15681.87	2223
	T_{run} (min)	2.94	504
	Mem (GB)	1.42	18.71

Table 2: Velocity results and Performance comparison of the two numerical approaches.

4.2 Comparison with analytical disperse result

The 3D fast Fourier transform (FFT) algorithm is used to perform the wavenumber analysis of time-domain signals, in order to compare computational wavefields from developed fast-FEM code and analytical SMM solutions for each propagation direction. Fig. 7 shows the calculated wavenumber domain signals in colormap and the SMM results in solid lines. The peak in the color bar is related to the wave amplitude and normalized by the maximum. There are no obvious peaks under the S0 curves, as the normal incidence under low frequency-thickness product mainly actuates the A0 wave. The fast-FEM results and the analytical SMM curves overlap well for the A0 Lamb waves, confirming the reliability of the model in each direction.

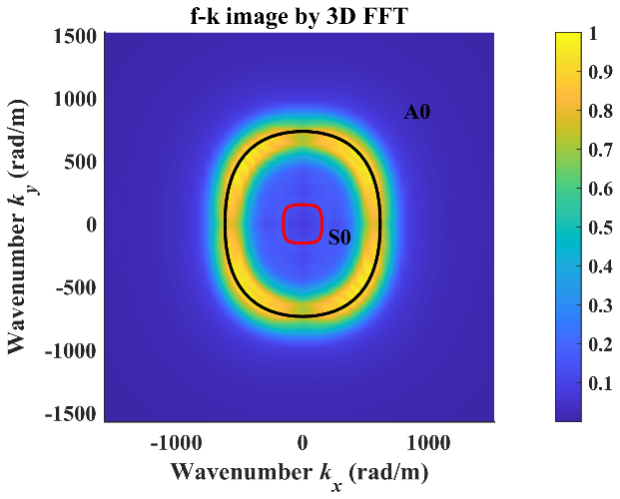

Figure 7: The wavenumber domain signals in colormap and the SMM results in solid lines.

4.3 Predicted signal and experiment validation

Based on the proposed fast FEM-based program, a model with the same dimension as the experiment plate is established. The actuator is simplified as a normal incidence in a 30 mm × 30 mm area. 31×31points are set in the sensor area with a spacing of 1 mm, and the integral of the signals is used to predict the signals generated by the actuator. The simulated wave field at a time of 54 μs is shown in Fig. 8. The amplitude of the particle oscillation displacement is denoted in the grayscale color bar. Both A0 mode and S0 mode can be distinguished, although the amplitude of the S0 mode is much smaller. The measured signal by experiment and the predicted signal from the simulation are shown in Fig. 9. The piezoceramic plates are sensitive to the out-of-plane motion; however, the measured signal is closer to the predicted in-plane signal compared to the out-of-plane displacement. The main reason is that the induced additional stiffness and similar thickness of the sensor/actuator to the plate result in the mode conversion, which could be reduced by other generation and detection approaches. The predicted model can also be improved by adding a sensor/actuator to the model, which would be further studied. However, it has been demonstrated that the proposed program could predict the arrival time and waveform signals of experiments, as shown in Fig. 9.,

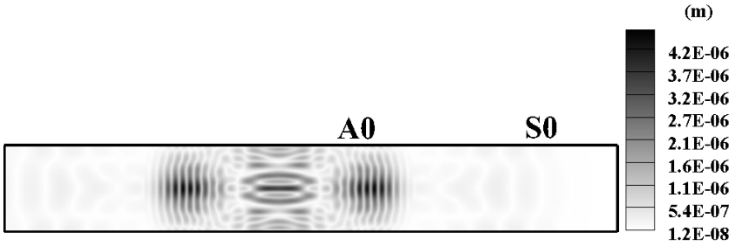

Figure 8: The simulated wave field of the GFRP plate used in experiment.

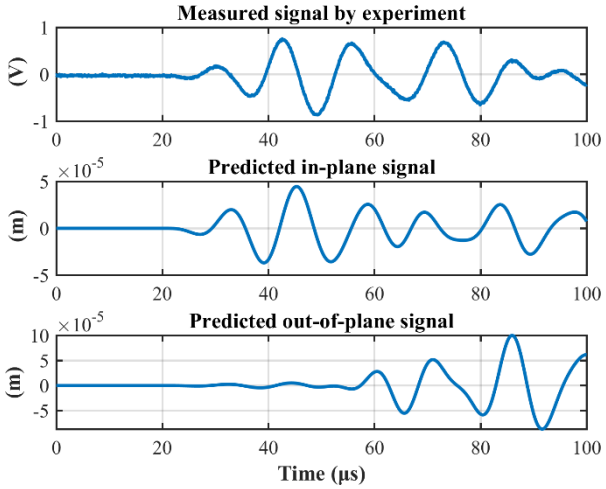

Figure 9: Measured signal and predicted signal.

5 CONCLUSIONS

In this paper, a fast FEM-based numerical program is established to simulate the guided wave propagation in composite plates. Combing the time-explicit algorithm and one-dimensional compressing data storage technique, the memory and computational costs are highly reduced. The method is applied to simulate guided waves in a glass fiber-reinforced polymer cross-ply laminate. Firstly, the analytical disperse solution in multi-layers plates is obtained based on the stiffness matrix method (SMM) with the assumption of transversely isotropic in each ply. Then, the COMSOL/Explicit package is used to simulate the same model as the fast FEM-based simulation. The results from both the two models are in good agreement with the theoretical values. With 7 times DoF more than commercial software, the storage capacity is 10 times less. And the calculation running time of the proposed method is only several minutes, while requires many hours in the commercial software. The results show that the proposed method offers a significant reduction in computation time and storage capacity, making it an efficient and reliable tool for simulating guided waves in composites.

Afterward, the accuracy of the fast FEM-based method for each propagation direction is verified with the comparison to analytical disperse solutions by wavenumber analysis. The fast-FEM results and the analytical SMM curves overlap well for the A0 Lamb waves, confirming the reliability of the model in each direction. Finally, the predicted signal from the proposed method is validated by experiments. The arrival time and waveform agree well with the signals. It shows that this efficient and reliable numerical approach could provide theoretical and technological support to guided waves-based structural health monitoring in composites.

ACKNOWLEDGEMENTS

The support provided by China Scholarship Council (CSC) during a visit of Xing KOU to Politecnico di Milano is acknowledged.

REFERENCES

[1] Z. Su, L. Ye and Y. Lu, Guided Lamb waves for identification of damage in composite structures: A review, *Journal of Sound and Vibration*, **295**, 2006, pp. 753–780 (doi: 10.1016/j.jsv.2006.01.020).

[2] B. Ren and C. J. Lissenden, Ultrasonic guided wave inspection of adhesive bonds between composite laminates, *International Journal of Adhesion and Adhesives*, **45**, 2013, pp. 59–68 (doi: 10.1016/j.ijadhadh.2013.04.001).

[3] Z. Tian, Lingyu Yu, C. Leckey and J. Seebo, Guided wave imaging for detection and evaluation of impact-induced delamination in composites, *Smart Materials and Structures*, **24**, 2015, p. 105019 (doi: 10.1088/0964-1726/24/10/105019).

[4] N. Rauter, R. Lammering and T. Kühnrich, On the detection of fatigue damage in composites by use of second harmonic guided waves, *Composite Structures*, **152**, 2016, pp. 247–258 (doi: 10.1016/j.compstruct.2016.05.049).

[5] F. Hervin and P. Fromme, Guided wave propagation and scattering at composite delaminations, *Proceedings of SPIE, Health Monitoring of Structural and Biological Systems XV*, **11593**, 2021, pp. 149–156 (doi: 10.1117/12.2582363).

[6] A. H. Orta, M. Kersemans and K. Van Den Abeele, A comparative study for calculating dispersion curves in viscoelastic multi-layered plates, *Composite Structures*, **294**, 2022, p. 115779 (doi: 10.1016/j.compstruct.2022.115779).

[7] L. Maio and P. Fromme, On ultrasound propagation in composite laminates: advances in numerical simulation, *Progress in Aerospace Sciences*, **129**, 2022, p. 100791 (doi: 10.1016/j.paerosci.2021.100791).

[8] F. Hervin, L. Maio and P. Fromme, Guided wave scattering at a delamination in a quasi-isotropic composite laminate: Experiment and simulation, *Composite Structures*, **275**, 2021, p. 114406 (doi: 10.1016/j.compstruct.2021.114406).

[9] H. Mei and V. Giurgiutiu, Characterization of multilayer delaminations in composites using wavenumber analysis: numerical and experimental studies, *Structural Health Monitoring*, **20**, 2021, pp. 1004–1029 (doi: 10.1177/1475921720939616).

[10] C. A. C. Leckey, K. R. Wheeler, V. N. Hafiychuk, H. Hafiychuk and D. A. Timuçin, Simulation of guided-wave ultrasound propagation in composite laminates: Benchmark comparisons of numerical codes and experiment, *Ultrasonics*, **84**, 2018, pp. 187–200 (doi: 10.1016/j.ultras.2017.11.002).

[11] A. De Luca, D. Perfetto, A. Polverino, A. Aversano and F. Caputo, Finite Element Modeling Approaches, Experimentally Assessed, for the Simulation of Guided Wave Propagation in Composites, *Sustainability*, **14**, 2022 (doi: 10.3390/su14116924).

[12] F. H. Quintanilla and C. A. C. Leckey, Lebedev scheme for ultrasound simulation in composites, *Ultrasonics*, **86**, 2018, pp. 28–40 (doi: 10.1016/j.ultras.2018.01.013).

[13] H. Chen, Z. Feng, Y. Du, Q. Chen and H. Miao, Spectral finite element method for efficient simulation of nonlinear interactions between Lamb waves and breathing cracks within the bi-potential framework, *International Journal of Mechanical Sciences*, **215**, 2022, p. 106954 (doi: 10.1016/j.ijmecsci.2021.106954).

[14] C. A. C. Leckey, M. D. Rogge and F. Raymond Parker, Guided waves in anisotropic and quasi-isotropic aerospace composites: Three-dimensional simulation and experiment, *Ultrasonics*, **54**, 2014, pp. 385–394 (doi: 10.1016/j.ultras.2013.05.007).

[15] A. H. Nayfeh and D. E. Chimenti, Free Wave Propagation in Plates of General Anisotropic Media, *Journal of Applied Mechanics*, **56**, 1989, pp. 881–886 (doi: 10.1115/1.3176186).

[16] A. H. Nayfeh, *Wave propagation in layered anisotropic media: with applications to composites*, Amsterdam New York: Elsevier, 1995.

[17] A. Kamal and V. Giurgiutiu, Stiffness Transfer Matrix Method (STMM) for stable dispersion curves solution in anisotropic composites, *Proceedings of SPIE, Health Monitoring of Structural and Biological Systems 2014 (Ed. T. Kundu), San Diego, California, USA*, **9064**, 2014, p. 906410 (doi: 10.1117/12.2044789).

[18] J. Ghaboussi and X. S. Wu, *Numerical Methods in Computational Mechanics*, Boca Raton: CRC Press, 2017 (doi: 10.1201/9781315368689).

[19] Y. Wu, C. Pei, H. Zhang, Y. Liu and P. Jia, A Fast Finite Element Simulation Method of Phased Array Ultrasonic Testing and Its Application in Sleeve Fillet Weld Inspection, *Applied Sciences*, **12**, 2022, p. 5384 (doi: 10.3390/app12115384).